

Numerical Simulation of Fluid Flow in Random Granular Porous Media using Lattice Boltzmann Method

M. M. Keshtkar*

Department of Mechanical Engineering,
Kerman Branch, Islamic Azad University, Iran
E-mail: mkeshtkar54@yahoo.com

*Corresponding author

Received: 2 March 2016, Revised: April 2016, Accepted: 23 May 2016

Abstract: In this paper, fluid flow between two parallel flat plates that are partially filled with two-dimension porous media is investigated numerically using single relaxation time (SRT) lattice Boltzmann method (LBM) at pore scale. The considered obstacles are random, circular, rigid and granular with uniform diameters. Single component and single-phase viscous Newtonian fluid are considered as working fluid. There are no overlaps between obstacles. It supposed incompressible, steady and laminar flow and no chemical reaction performed in porous media. Velocity vectors and streamlines in this domain depicted. The effect of varying Reynolds number on the pressure drop or pressure gradient and Darcy drag are studied. Dimensionless permeability calculated as a function of porosity and Knudsen number. To vary porosity, obstacles diameter changed but their places considered constant. With increasing Knudsen number, the dimensionless permeability is increased. In addition, effect of domain resolution on pressure gradient investigated. The results demonstrate that lattice Boltzmann method will be very useful in fluid flow simulation through porous media.

Keywords: Darcy law, Lattice boltzmann method, Lid porous media, Permeability, Pore scale

Reference: Keshtkar, M. M., “Numerical Simulation of Fluid Flow in Random Granular Porous Media using Lattice Boltzmann Method”, *Int J of Advanced Design and Manufacturing Technology*, Vol. 9/No. 3, 2016, pp. 31-40.

Biographical notes: **M. M. Keshtkar** received his PhD in Mechanical Engineering from Islamic Azad University, Science and Research Branch, in 2009. He is currently Assistant Professor at the Department of Mechanical Engineering, Kerman University, Kerman, Iran.

1 INTRODUCTION

In fluid flow analysis three views exist: microscopic (Liouville equation), mesoscopic (particle kinetic equation) and macroscopic view (Navier–Stokes equations). In microscopic view, single particle motion is studied (molecular dynamics). This modeling method for solving engineering problems is very time consuming and not cost effective. Mesoscopic view is between microscopic and macroscopic views and instead of a single molecule investigation, a set of molecules (named molecular parcel) are considered as a particle (statistical thermodynamics). All molecules in a parcel have velocities $U+dU$, $V+dV$ and $W+dW$. Lattice Boltzmann method (LBM) is one of the most important mesoscopic methods in fluid flow simulation. Since three previous decades, LBM is converted to a powerful and useful method in computational fluid dynamics (CFD) and nowadays LBM is an excellent alternative for conventional CFD (finite difference, finite volume and finite element) especially multi-phase and multi component flows in complex geometries and porous media. In LBM simulation instead of solving Navier–Stokes equations, the discrete lattice Boltzmann equation (LBE) is solved to simulate the Newtonian fluid flow with collision operator models such as Bhatnagar-Gross-Krook (BGK approximation). Since Navier–Stokes equations are nonlinear partial differential equations but LBE is a first order linear partial differential equation, so its discretization and computer programming is more convenient. Fluid flow through porous media is very applicable in industry for example, in mechanic engineering such as in filters and filtration, acoustics, heat recovery systems, radiant burner, etc., in civil engineering such as underground water, water drainage, soil mechanics, rock mechanics, hydrogeology, etc. In chemical engineering such as chromatography method in separation of different fluid, in medical sciences such as biology and biophysics and in another sciences for example, geophysics and material science.

A porous media is a material containing void spaces or pores (spaces between solid materials) that liquid or gas can pass through it. The skeletal portion of the material often is called the matrix. The voids typically are filled with a fluid and fluid can pass through media. The skeletal material is usually rigid or deformable. Obstacles can be fixed or in motion. In this study, rigid obstacles are considered. A porous media often is characterized by its porosity. Other properties of the media (e.g. permeability, tensile strength, electrical conductivity) can sometimes be derived from the respective properties of its constituents (solid matrix and fluid) and the media porosity and pores structure. Porosity is an essential factor in filtering process in industry so that particles must be removed by a porous medium.

The pores must be small enough in such that effectively trap foreign particles. rocks, soil, bones, wood, cork, some types of stone, such as sandstone, artificial materials such as

cements, sponges, reticulated foam and ceramics can be considered as porous media. Permeability calculation is very important in porous media studying. In fact permeability is the media ability for passing fluid. Spaid and Phelan [1] studied lattice Boltzmann methods for modeling micro scale flow in fibrous porous media. They concluded that LBM is equivalent for solving a hybrid method of the Stokes and Brinkman equations, where the Brinkman equation is applied to model flow through porous media, while the Stokes equation is applied to the open regions outside the porous media.

Bernsdorf et al. [2] investigated the pressure drop in porous media flow with LBM. They concluded at the low Reynolds number in regularly packed beds of spheres, LBM is able to quantitatively predict pressure drop with high accuracy. Abdussamie [3] surveyed Navier-Stokes solutions for flow and transport in realistic porous media. He used both finite-element and finite volume methods, for solving Navier-Stokes equations and showed that, COMSOL solver has a good agreement with CFD FLUENT solver. Thompson and Fogler [4] modeled flow in disordered packed beds at pore-scale. They showed the pore-scale analysis provides a quantitative match with experimental macroscopic transport parameters. Van Doormaal and Pharoah [5] determined the permeability of fibrous porous media using the LBM with application to PEM fuel cells. They showed that the LBM can be used to determine the permeability in an idealized porous transport layer (PTL). Also they found relationships between permeability, porosity and fiber angle for fibrous porous media.

Pazdriakou and Adler [6] determined dynamic permeability of porous media by the LBM. They imposed an oscillating macroscopic pressure gradient to generate oscillating flows. They concluded that the Knudsen number has a crucial influence on the numerical precision for low frequencies and for obtaining accurate results, Kn number must be small. Golestanian [7] determined the permeability variation with porosity for composite performs experimentally. All of his experiments were done under constant pressure conditions and RL-440 Epoxy resin was used as the working fluid. He showed that the permeability increases sharply as porosity increases above a certain value.

Despois and Mortensen [8] surveyed the permeability of open-pore microcellular materials. They showed experimental data agrees with other data reported in the literature. Martys et al. [9] studied universal scaling of fluid permeability for sphere packing. They simulated Stokes flow through random packing of spheres with and without overlap and submitted universal curves for permeability such that one need only know the specific area and critical porosity then refer to their submitted universal curves, for evaluate permeability. Ngo and Tamma [10] predicted complex three-dimensional micro structural permeability of porous fibrous media with and without compaction. They studied realistic complex fabric geometries and structural

shapes and proposed using a three-dimensional unit cell to predict permeability.

Nabovati et al. [11] surveyed three dimensional fluid flow simulations in fibrous media using the SRT lattice Boltzmann method. They concluded that fiber curvature has a negligible impact on the media permeability. Chai et al. [12] investigated non-Darcy flow in disordered porous media with high porosity. They showed that non-Darcy effect is observed obviously, when Reynolds number is up to a critical value. Gao et al. [13] calculated permeability of anisotropic porous media. They compared the SRT lattice Boltzmann method with multi relaxation time (MRT), and showed that although MRT model is an improved method, the SRT method is more competitive by properly choosing the value of the relaxation time. Cho et al. [14] studied permeability of micro scale fibrous porous media using LBM. They showed that the fibrous porous media behaves as the granular porous media at low porosities. Grucelski and Pozorski [15] simulated flow in simple porous media. They obtained lift and drag coefficients and the Strouhal number as the functions of the Reynolds number. Also they showed that according to porous media theory, the pressure drop meets the Darcy law for low Reynolds numbers and for higher Reynolds number, it is better to apply a quadratic polynomial (the Darcy–Forchheimer law). Zarghami et al. [16] studied the porous media with non-homogeneous porosity with a finite volume combined with Lattice Boltzmann method [FVM-LBM]. They also investigated the effects of Darcy number, porosity and porous layer thickness at canal walls. When Darcy number or media porosity is high, they showed that the fluid flows more easily through the porous layer at walls. Anisotropic porous media behavior was studied by Deshpande et al. [17]. They simulated flow through porous media with varying degrees of anisotropy. Ortega and Romo investigated simulation of a non-Newtonian fluid in porous media [18]. They found that in random porous media there is flow separation. In this work, fluid flow through random circular porous media between two parallel flat plates is studied. Pressure drop along porous media, velocity vectors and streamlines are depicted. The effect of porosity and Knudsen number on permeability is also analyzed.

2 THEORETICAL ANALYSIS

2.1 LATTICE BOLTZMANN METHOD

Nowadays, the lattice Boltzmann method (LBM) has been developed into an alternative numerical method for CFD in simulating fluid flows [19-21, 30, 31]. The earliest Lattice Boltzmann method was generated to solve one of the main problems of lattice gas automata (LGA) method; that is, statistical noise [22, 23]. For more details on LGA method, one can refer to ref [20, 24]. In this work, the lattice Boltzmann method with two-dimensional single relaxation time (SRT) [19] has been applied. In LBM, Macroscopic

properties and parameters of fluid as a continuum environment in basis of microscopic properties and parameters were obtained. For D2Q9 model (nine-speed model), the lattice velocities are shown at Fig. 1.

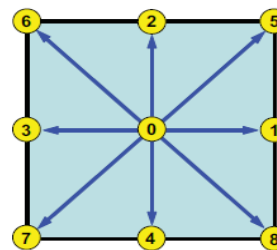


Fig. 1 The D2Q9 model with discrete velocities

Bhatnagar-Gross-Krook in 1954 introduced a discrete form for Boltzmann equation and suggested BGK approximation as follows:

$$f_{\alpha}(\mathbf{x} + \mathbf{e}_{\alpha}\delta t, t + \delta t) = f_{\alpha}(\mathbf{x}, t) - \frac{f_{\alpha} - f_{\alpha}^{eq}}{\tau} \quad (1)$$

Where f_{α} is the distribution function and is a non-negative scalar variable between 0 and 1 for particles prediction. \mathbf{x} and t are particles coordinates and time, δt is time step in lattice. We select $\delta t = \delta x = 1$ for ease of calculation. \mathbf{e}_{α} is the lattice velocity namely $\mathbf{e}_{\alpha} = \frac{\delta \mathbf{x}}{\delta t}$ and α is number

of directions in lattice. Lattice velocities are always constant but macroscopic velocities U , V and W , are variables. The Eq. (1) splits in to two steps: collision and streaming (or propagation). In streaming step, each particle moves to the nearest adjacent node in the direction of its discrete velocity \mathbf{e}_{α} . Collision occurs when particles arrives at a same node and at this node, collision happens. Collision step is considered as a relaxation towards a local equilibrium. It should be noted that collision step is performed completely locally and independent of particle coordinates and also streaming step has very low computational cost in programming.

Collision step:

$$\tilde{f}_{\alpha}(\mathbf{x}, t) = f_{\alpha}(\mathbf{x}, t) - \frac{1}{\tau} [f_{\alpha}(\mathbf{x}, t) - f_{\alpha}^{(eq)}(\mathbf{x}, t)] \quad (2)$$

Streaming step:

$$f_{\alpha}(\mathbf{x} + \mathbf{e}_{\alpha}\delta t, t + \delta t) = \tilde{f}_{\alpha}(\mathbf{x}, t) \quad (3)$$

Where \tilde{f} , is the post-collision distribution function and f_{α}^{eq} is the equilibrium distribution function (Maxwell-Boltzmann distribution) which are originated from the

maximum entropy principle and are calculated from Eq. (4). τ is the dimensionless relaxation time.

$$f_{\alpha}^{eq} = \rho w_{\alpha} \left[1 + 3e_{\alpha} \mathbf{u} + \frac{9}{2} (e_{\alpha} \mathbf{u})^2 - \frac{3}{2} u^2 \right] \quad (4)$$

Where w_{α} is the weighting factor which are used for discretization of Maxwell-Boltzmann equilibrium distribution and given by:

$$w_{\alpha} = \begin{cases} 4/9, & \alpha = 0, \\ 1/9, & \alpha = 1,3,5,7, \\ 1/36, & \alpha = 2,4,6,8. \end{cases} \quad (5)$$

In the discrete velocity space, the fluid density and velocity can be evaluated as follows:

$$\begin{aligned} \rho &= \sum_{\alpha=0}^8 f_{\alpha} = \sum_{\alpha=0}^8 f_{\alpha}^{(eq)} \\ \mathbf{u} &= \frac{1}{\rho} \sum_{\alpha=1}^8 e_{\alpha} f_{\alpha} = \frac{1}{\rho} \sum_{\alpha=1}^8 e_{\alpha} f_{\alpha}^{(eq)} \end{aligned} \quad (6-7)$$

Fluid kinematic and dynamic viscosity (ν and μ respectively) in LBM scale are the functions of relaxation time τ and in the D2Q9 model are given by Eq. (8-9).

$$\begin{cases} \nu = (\tau - \frac{1}{2}) c_s^2 \delta t \\ \mu = \frac{\rho}{3} \left(\tau - \frac{1}{2} \right) \end{cases} \quad (8-9)$$

Where c_s is the sound speed that in D2Q9 model is $c_s = e/\sqrt{3}$. Fluid pressure in D2Q9 model is obtained from Eq. (10) which is similar to equation of state for gas. According to Eq. (8), since the negative viscosity is physically meaningless, it is necessary to always select $\tau \geq 1/2$. This inequality is stability condition for LBM.

$$P = \frac{\rho}{3} \quad (10)$$

Mach number is defined according to Eq. (11).

$$Ma = \frac{u}{c_s} \quad (11)$$

Compressibility is measured with Mach number. In LBM it is assumed that fluid compressibility is low. For incompressible flow simulation with LBM, it is necessary to reduce the fluid compressibility with reducing Mach number. The numerical accuracy of LBM depends on Mach number. Compressibility effects are negligible by choosing the Mach number below 0.1 and flow can be considered as a quasi-incompressible flow. Usually two scales have been used in lattice Boltzmann simulation of fluid flow in porous

media; the pore scale and the representative elementary volume (REV) scale [25]. In the pore scale, the porous media geometry is simulated exactly and porous media effect on flow is modeled only by the no-slip bounce-back boundary condition. In the REV scale, the porous media effect on flow is modeled by an additional term (body force) that is added to the lattice Boltzmann equation. The pore scale is the easiest approach to apply the LBM to porous flows [26]. In this paper, simulation of fluid flow in porous media at pore scale is considered.

2.2 Boundary condition

At each node, unknown distribution functions (f) in terms of known distribution functions are expressed. According to Fig. 2 at inlet, f_1 , f_5 and f_8 and at outlet, f_3 , f_6 and f_7 are unknown.

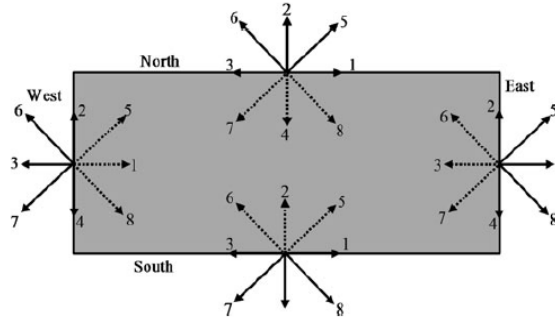


Fig. 2 Known (solid line) and unknown (dashed line) distribution functions at boundaries [21]

At inlet, with having inlet velocity and fluid density, three unknown distribution functions were obtained and known velocity boundary condition (Zhu and He) at inlet were used as follows:

$$\rho_{in} = \frac{[f_0 + f_2 + f_4 + 2(f_3 + f_6 + f_7)]}{1 - u_{x \text{ in}}} \quad (12)$$

$$\begin{aligned} f_1 &= f_3 + \frac{2}{3} (\rho u)_{in} \\ f_5 &= f_7 + \frac{1}{2} (f_4 - f_2) + \frac{1}{6} (\rho u)_{in} \end{aligned} \quad (13-14)$$

$$f_8 = f_6 + \frac{1}{2} (f_2 - f_4) + \frac{1}{6} (\rho u)_{in}$$

At outlet, second order polynomial extrapolation is used (Eq. (16-18)). This approach is similar to the approach used in traditional finite difference methods (FDM) for boundary conditions.

$$\begin{cases} f_3^{N_x} = 2f_3^{N_x-1} - f_3^{N_x-2} \\ f_6^{N_x} = 2f_6^{N_x-1} - f_6^{N_x-2} \\ f_7^{N_x} = 2f_7^{N_x-1} - f_7^{N_x-2} \end{cases} \quad (16-18)$$

Where, N_x is the nodes number in x direction. Because of no slip condition in solid walls, the on grid bounce-back boundary condition was used at lower and upper walls of canal. This model is the simplest model that satisfies no slip condition at fluid-solid interface. In bounce-back model, it assumed when a particle reaches wall, the particle would bounce back to the fluid nodes along its incoming direction. According to Fig. 2 at upper wall, f_4, f_7 and f_8 and at lower wall, f_2, f_5 and f_6 are unknown that are obtained from Eq. (19).

$$f_{\bar{\alpha}}(x_f) = f_{\alpha}(x_f) \tag{19}$$

Where :

$$e_{\bar{\alpha}} = -e_{\alpha} \tag{20}$$

and x_f is the fluid node at lower and upper walls of canal.

2.3 Curved boundary

At Fig. 3, a curved boundary is shown that separates fluid and solid region from each other's. Solid, fluid and wall nodes are shown with x_b, x_f and x_w respectively. Wall nodes result from intersecting curved boundary with lattice. At the curved walls of obstacles, linear interpolation method (Δ fraction) [27] is used. Particle velocity from x_f to x_b is e_{α} and from x_b to x_f is $e_{\bar{\alpha}}$. According to Fig. 3 the streaming step requires the information of $\tilde{f}_{\bar{\alpha}}(x_b, t)$ on the solid side in order to obtain $f_{\bar{\alpha}}(x_f, \delta t)$ for the fluid node at x_f .

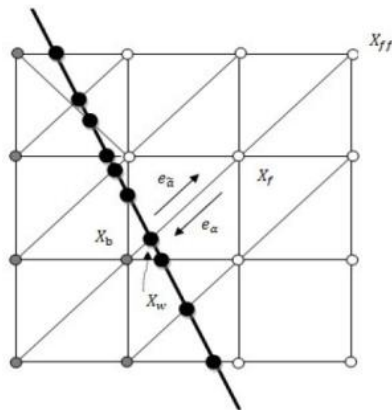


Fig. 3 Curved boundary on the lattice

With defining:

$$\Delta = \frac{|x_f - x_w|}{|x_f - x_b|}, 0 \leq \Delta \leq 1 \tag{21}$$

When fluid nodes are located on the wall, $\Delta = 0$. $\tilde{f}_{\bar{\alpha}}(x_b, t)$ is unknown which Mei et al. [27] proposed linear interpolation (Eq. (22)) for this term.

$$\tilde{f}_{\bar{\alpha}}(x_b, t) = (1 - \chi)\tilde{f}_{\alpha}(x_f, t) + \chi f_{\alpha}^{(*)}(x_b, t) + 2w_{\alpha}\rho \frac{3}{e^2} e_{\bar{\alpha}} \cdot u_w \tag{22}$$

With

$$f_{\alpha}^{(*)}(x_b, t) = w_{\alpha}\rho(x_f, t) \left[1 + \frac{3}{e^2} e_{\alpha} \cdot u_{bf} + \frac{9}{2e^4} (e_{\alpha} \cdot u_f)^2 - \frac{3}{2e^2} u_f \cdot u_f \right] \tag{23}$$

$$u_{bf} = \left(\frac{\Delta - 1}{\Delta} \right) u_f + \frac{u_w}{\Delta} \text{ and } \chi = \frac{2\Delta - 1}{\tau} \text{ for } \Delta \geq 1/2. \tag{24}$$

$$u_{bf} = u_{ff} = u_f(x_f + e_{\alpha}\delta t, t) \text{ and } \chi = \frac{2\Delta - 1}{\tau - 2} \text{ for } \Delta < 1/2. \tag{25}$$

Where u_w is the curved wall (boundary) velocity, that in this work $u_w = 0$ namely the obstacles are fixed and do not move. χ is the weighting factor that is a function of Δ and controls the linear interpolation. u_{bf} is a virtual velocity and $f_{\alpha}^{(*)}$ is the virtual equilibrium distribution function.

2.4 Flow in porous media

The momentum equation for fluid flows passing through a porous media described by Darcy law [28, 29]

$$u = -\frac{K}{\mu} \frac{\partial p}{\partial x} \tag{26}$$

Where u is velocity, $\frac{\partial p}{\partial x}$ is the pressure gradient in the flow

direction, μ is the dynamic viscosity of the fluid and K is the permeability tensor of the media. For an isotropic media, this tensor reduces to a scalar.

3 METHOD OF SOLUTION

Validation of base computer code done with Poiseuille fully developed laminar flow (without porous media) between two parallel flat plates. The exact solution is:

$$u = \frac{1}{2\mu} \left(\frac{\partial p}{\partial x} \right) y^2 - \frac{1}{2\mu} \left(\frac{\partial p}{\partial x} \right) Hy = \frac{H^2}{2\mu} \left(\frac{\partial p}{\partial x} \right) \left[\left(\frac{y}{H} \right)^2 - \left(\frac{y}{H} \right) \right] \tag{27}$$

Where H is the distance between plates and y is measured from down plate. Dimensionless velocity profile is:

$$\frac{u}{\bar{u}} = 6 \left[\frac{y}{H} - \left(\frac{y}{H} \right)^2 \right] \quad (28)$$

Where \bar{u} is the mean velocity. As shown in Fig. 5 LBM results match with analytical solution with a good precision. Velocity at walls becomes zero and maximum velocity is obtained at centerline. Maximum velocity is obtained with absolute error of 5.4120×10^{-7} that is very small and negligible. Hence, LBM numerical solution has very good coincidence with analytical solution.



Fig. 4 The Schematic of a canal with H distance.

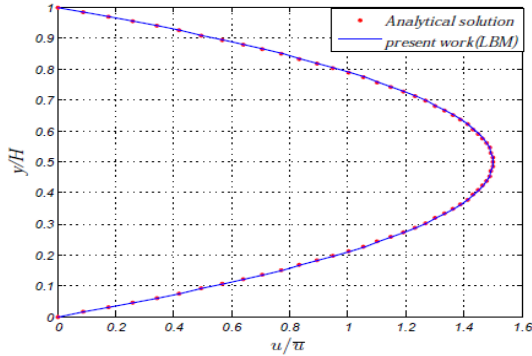


Fig. 5 Dimensionless velocity profile in Poiseuille flow

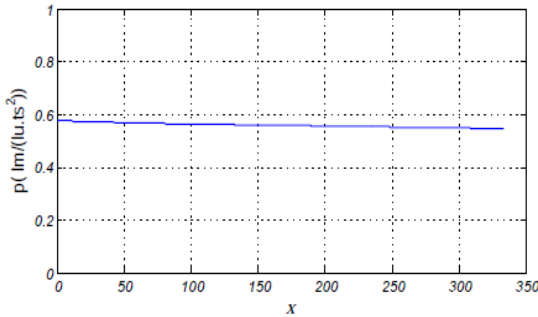


Fig. 6 Linear pressure drop along centerline in Poiseuille flow

In Fig. 6 fluid pressure drops at Poiseuille flow along canal centerline in LBM scale is drawn. As shown in Fig. 6 and according to Eq. (29) pressure drop is linear.

$$\Delta p = - \frac{12 \mu \bar{u} \Delta x}{H^2} \quad (29)$$

4 RESULTS AND DISCUSSION

General layout of porous media is shown in Fig. 7 in which D_p is the obstacles diameter. All particles have same diameter.

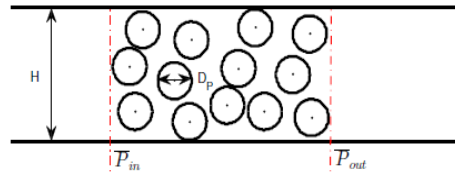


Fig. 7 Schematic of a random circular porous media

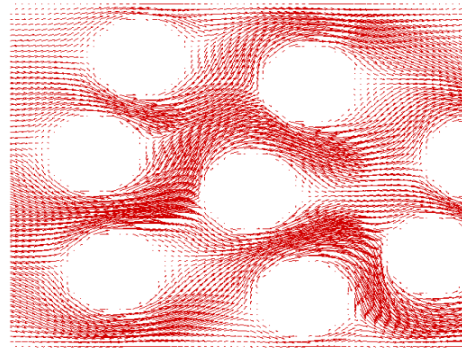


Fig. 8 Velocity vectors in porous media at $Re_H = 40$, $Re_{D_p} = 8.4$ and porosity 0.72

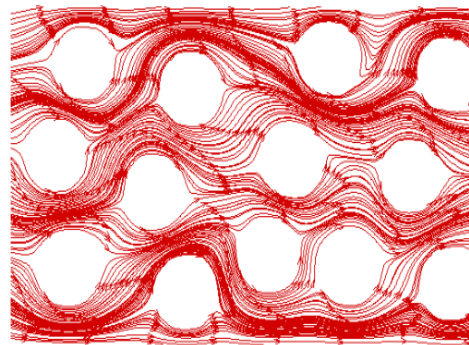


Fig. 9 Stream lines in porous media at $Re_H = 40$, $Re_{D_p} = 8.4$ and porosity 0.72

To show the effect of the porous media on flow, in Fig. 8 and Fig. 9, velocity vectors and streamlines are drawn with Techplot software at $Re_H = 40$, $Re_{D_p} = 8.4$ and porosity of 0.72. Obstacles diameter are 14 lu (lattice unit) or 0.47 cm. Canal length L is 0.1 m and inlet velocity is $u_0 = 0.1 lu/ts$. As Fig. 8 shows, velocity vectors turn the obstacles and velocity inside obstacles is zero. Because of no permeation condition, there are not any velocity vectors inside obstacles as shown in Fig. 8.

3.2.1 Pressure drop calculations

In Fig. 10 effect of Reynolds number based on the particle diameter Re_{D_p} on the mean pressure drop is depicted. The mean pressure drop is calculated as follows:

$$\Delta \bar{p} = \bar{p}_{out} - \bar{p}_{in} \quad (30)$$

In which \bar{p}_{in} and \bar{p}_{out} are fluid mean pressure at cross section right before and after porous media respectively. These two cross-sections are shown in Fig. 7. Mean pressure is calculated according to Eq. (31).

$$\bar{p} = \frac{\sum_{i=1}^{N_y} p_i}{N_y} \quad (31)$$

Where N_y is lattice nodes number in y direction (porous media width) and in this study is constant and equals to 67 nodes.

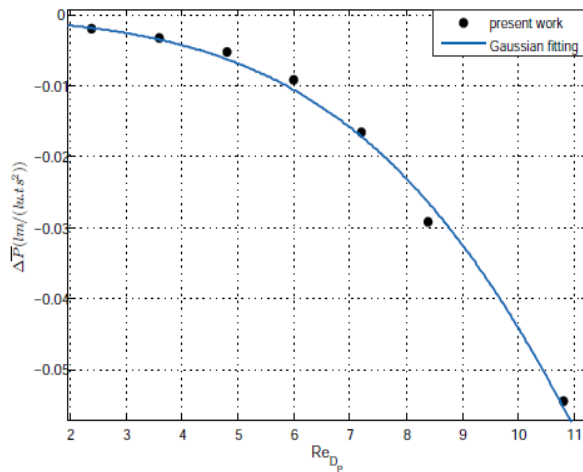


Fig. 10 Mean pressure drop vs. Re_{D_p}

As shown in Fig. 10 with increasing Reynolds number Re_{D_p} (for example with an increase in obstacles diameter), fluid pressure drop along the porous media increases and becomes more negative. When Re_{D_p} increases by an increasing in obstacles diameter, contact surface of obstacles increases and because of friction between fluid and obstacles, fluid pressure reduces, pressure drop increase and become more negative. In Fig. 11 effect of Re_{D_p} on pressure gradient along the porous media is plotted. Pressure gradient is calculated according Eq. (32).

$$\nabla \bar{p} = \frac{\Delta \bar{p}}{\Delta x} = \frac{\bar{p}_{out} - \bar{p}_{in}}{\Delta x} \quad (32)$$

3.2.2 Permeability and porosity

In fluid dynamics, the ratio of the molecular mean free path l to characteristic length h is defined as Knudsen number that is a dimensionless number [14]. The chosen characteristic length will depend on the problem under consideration. It may be, for example, the diameter of a pipe or an obstacle immersed in a flow, or the thickness of a boundary layer. This number was named after Danish physicist Martin Knudsen (1871–1949):

$$Kn = \frac{l}{h} \quad (33)$$

The mean free path l is the particle's distance traveled during the relaxation time λ with a lattice speed, e .

$$e = \frac{\delta x}{\delta t} \quad (34)$$

$$l = e \lambda = \frac{\delta x}{\delta t} \lambda = \tau \delta x \quad (35)$$

Where τ , is the dimensionless relaxation time and is equal:

$$\tau = \frac{\lambda}{\delta t} \quad (36)$$

So

$$Kn = \frac{l}{h} = \frac{\tau \delta x}{h} \quad (37)$$

With choosing $\tau = 1, \delta x = 1$, characteristic length h , is equal to particle diameter (D_p):

$$Kn = \frac{1}{D_p} \quad (38)$$

Small obstacles diameter is equal to large Kn number. In Fig. 12 dimensionless permeability as a function of Kn number is depicted. As shown in Fig. 12 when Kn number increases (namely obstacles become smaller) dimensionless permeability grows. With obstacles shrinking and with this assumption that obstacles position is constant, fluid can pass through porous media with more freedom and permeability of porous media increases. As previously mentioned permeability is a property of media and is independent of fluid. Therefore, when fluid changes, (viscosity) media permeability remains constant.

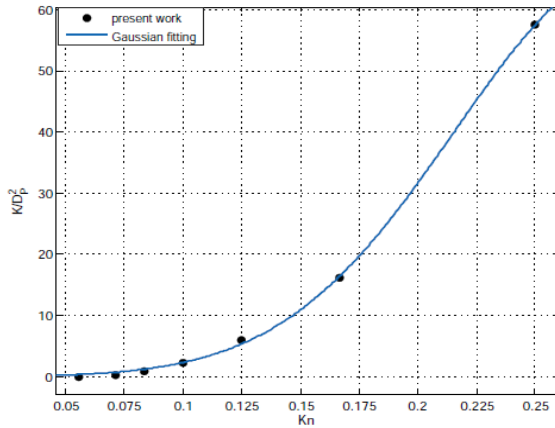


Fig. 12 Dimensionless permeability vs. Kn number

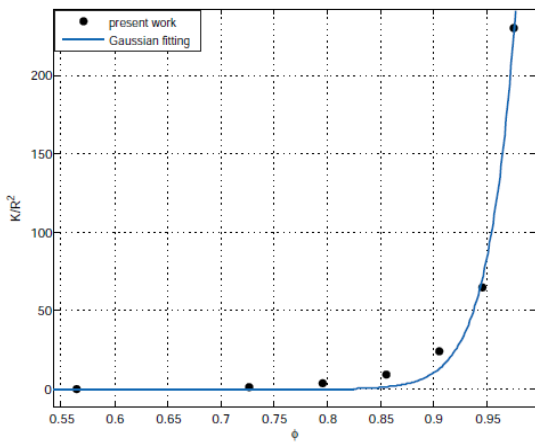


Fig. 13 Dimensionless permeability vs. porosity

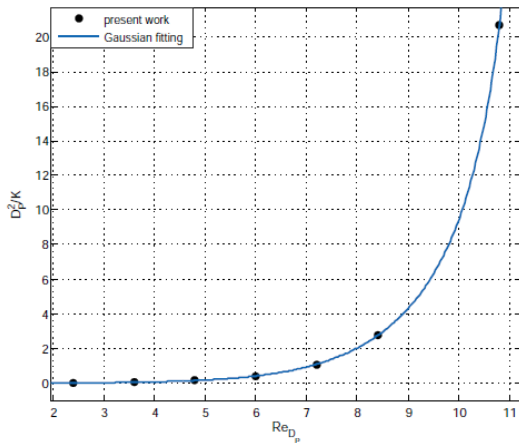
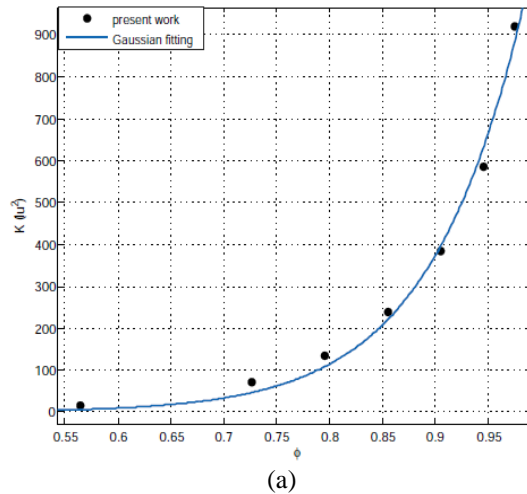


Fig. 14 Darcy-drag (inverse of dimensionless permeability) vs. Re_{D_p}

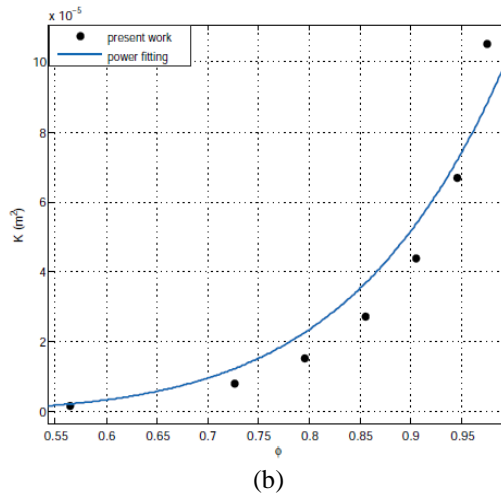
In Fig. 13 dimensionless permeability as a function of porosity is drawn. Since permeability has dimension of L^2 , we can normalize and dimensionless it with R_p^2 or D_p^2 term. If porosity increases, it means that void places increase and

fluid can flow through porous media easier thus media permeability will be increased.

In Fig. 14 effect of Re_{D_p} on Darcy drag (inverse of dimensionless permeability) is plotted. It should be noted that, Darcy drag is introduced in Darcy law with Forchheimer term. According to Fig. 14, when Re_{D_p} increases, Darcy-drag increases too, that means dimensionless permeability decreases. It should be noted that this ascending behavior is coincidence with results obtained from Chai et al. [12]. It concluded that for low porosities, growing of dimensionless permeability is slow.



(a)



(b)

Fig. 15 Permeability vs. porosity at LBM scale (a) and SI scale (b)

Fig. 15 Shows Permeability vs. porosity at LBM scale (a) and SI scale (b). In Fig. 15 permeability in LBM scale (lu²) and SI scale (m²) as a function of porosity is submitted. As shown in Fig. 15 with increasing porosity (with fixed obstacles and varying obstacles diameter), permeability also increases and at maximum porosity, maximum permeability is available. These results match with results of Deshpande

et al [17]. To change porosity, it is assumed in this work that obstacles location in channel is fixed and only diameter changes. Whatever porosity of porous media is larger, then fluid can pass through media easier and therefore permeability rises.

In general, permeability is a second order tensor (matrix) for anisotropic media but for an isotropic media, permeability in all directions is equal and this tensor will reduce to a scalar. Permeability is ability of a media for passing flow. K is not a function of fluid material (viscosity) but is a function of media geometry namely obstacle diameter. Therefore if fluid changes, K do not change. For natural porous media, porosity does not usually exceed 0.6. Artificial materials such as metallic foams, porosity can approach the value unit. For unit conversion of permeability from LBM scale (lu^2) to SI scale (m^2), Eq. (39) is used.

$$K_{SI} (m^2) = \delta^2 K_{LBM} (lu^2) \quad (39)$$

Where δ is conversion coefficient between two scales.

Table 1: Effect of resolution on mean pressure gradient

Lattice	D(lu)	D(m)	$\nabla \bar{P}_{LBM}$ (lm.lu-2.ts-2)
102 x 67	4	0.0013	-1.9115e-05
104 x 67	6	0.0020	-3.1470e-05
106 x 67	8	0.0027	-5.0331e-05
108 x 67	10	0.0033	-8.4587e-05
110 x 67	12	0.0040	-1.5016e-04
112 x 67	14	0.0047	-2.5831e-04
116 x 67	18	0.0060	-4.6526e-04

3.2.3 Resolution effect

Generally, for obtaining precise solution; the lattice must be fine with increasing lattice nodes. At the other hand for reducing calculations and saving time, the lattice do not should be very fine. Therefore, in a numerical simulation an agreement between high precision results and code speed is necessary and suitable nodes number should be selected. In Table 1 dependence of results (pressure gradient) to nodes number is studied and results show that this dependence is small. For unit conversion of diameter from LBM scale (lu) to SI scale (m), Eq. (40) is used.

$$D_{SI} (m) = \delta D_{LBM} (lu) \quad (40)$$

5 CONCLUDING REMARKS

In this paper single relaxation time (SRT) lattice Boltzmann method was used for fluid flow simulation in random circular porous media and ability of this numerical method was surveyed in complex geometries such as random porous media. In absence of porous media (Poiseuille flow between

two parallel plates), the obtained results from LBM match completely with analytical solution and dimensionless velocity profile as well as linear pressure drop along canal is depicted.

In Poiseuille flow, maximum velocity at centerline is obtained with absolute error of 5.4120×10^{-7} that is very small and negligible. Hence, LBM numerical solution has very good coincidence with analytical solution. Results show that porous media tend to raise pressure drop and fluid pressure decreases during pass porous media hence for handling fluid through porous media, more power is needed. With increasing obstacles number or their size, porosity reduces and pressure drop rises.

Pressure drop rising means pressure drop becomes more negative. Permeability was depicted in terms of porosity in both LBM and SI scales. With rising porosity, permeability rises. According to permeability versus porosity plot, it is concluded that materials with low porosity are less permeable and typically have smaller pores, making it more difficult for fluid to pass through them, while materials with high porosity have large pores and are easily permeated.

In addition, dimensionless permeability was plotted versus Kn number and porosity. With rising Knudsen number, dimensionless permeability rises. It is concluded that with increasing Reynolds number, Darcy-drag increased. With increasing Reynolds number, pressure drop and pressure gradient becomes more negative. In addition, effect of domain resolution on pressure gradient was investigated and it was observed that domain resolution has negligible effect on pressure gradient. Finally, it was found that the LBM is a useful, fast and accurate method for the investigation of fluid flows through porous media.

REFERENCES

- [1] Ghia, U., Ghia, K. N. and Shin, C. T., "High-Re solutions for incompressible flow using the Navier-Stokes equations and a multigrid method", J. Computational Physics, Vol. 48 ,1982, pp. 387-411.
- [2] Koseff, J. R. and Street, R. L., "The Lid-Driven Cavity Flow: A Synthesis of Qualitative and Quantitative Observations", J. Fluids Engineering, Vol. 106, 1984,, PP. 390-398.
- [3] Migeon, C., Pineau, G., and Texier, A., "Three-dimensionality development inside standard parallel pipe lid-driven cavities at $Re=1000$ ", J. Fluids and Structure, Vol. 17, 2003, PP. 717-738.
- [4] Ilegbusi, O. J. and Mat, M. D., "A comparison of predictions and measurements of kinematics mixing of two fluids in a 2D enclosure", App. Mathematical Modelling, Vol. 24, 2000, PP. 199-213.
- [5] Vogel, M. J., Hirs, A. H. and Lopez, J. M., "Spatio-temporal dynamics of a periodically driven cavity flow", J. Fluids Mechanics, Vol. 478, 2003, PP. 197-226.
- [6] Cortes, A.B., Miller, J. D., "Numerical experiments with the lid driven cavity flow problem", J. Computers and Fluids, Vol. 23, 1994, PP.1005-1027.
- [7] Fusegi, T., Hyun J. M., Kuwaharas, K. and Farouk B., "A numerical study of three dimensional natural convection in a

- differentially heated cubical enclosure", *Int. J. Heat Mass Transfer*, Vol. 34, 1991, PP. 1543-1557.
- [8] Barakos, G., Mitsoulis E., and Assimacopoulos D., "Natural convection flow in a square cavity revisited: laminar and turbulent models with wall functions", *Int. J. Numerical Methods Fluids*, Vol. 18, 1994, PP. 695-719.
- [9] Zhou, Y. C., "DSC solution for flow in a staggered double lid driven cavity", *Int. J. Numerical Methods in Engineering*, Vol. 57 2003, PP. 211–234.
- [10] Wu, J.S., Shao, Y.L., "Simulation of lid-driven cavity flows by parallel lattice Boltzmann method using multi-relaxation-time scheme", *Int. J. Numerical Methods in Fluids*, Vol. 46, 2004, PP. 921-937.
- [11] Siegmann, T., Schmidt, J.R. and Albensoeder, S., "Experiments on the flow stability in a double-lid-driven cavity", *PAMM*, Vol. 5 , 2005, PP. 551-552.
- [12] Albensoeder, S. and Kuhlmann, H.C., "Accurate three-dimensional lid-driven cavity flow", *J. Computational Physics*, 206 (2005), PP. 536-558.
- [13] Chen, C. L., "Numerical study of flow and thermal behavior of lid-driven flows in cavities of small aspect ratios", *Int. J. Numerical Methods in Fluids*, Vol. 52, 2006, PP. 785–799.
- [14] Leriche, E., "Direct Numerical Simulation in a Lid-Driven Cavity at High Reynolds Number", *Conference on Turbulence and Interactions*, 2006.
- [15] Rouse, D. R., "Numerical predictions of two-dimensional conduction, convection and radiation heat transfer- part 1", *Int. J. Thermal Science*, Vol. 39, 2000, PP. 315-331.
- [16] Rouse, D. R., Gautier, G. and Sacadura J. F., "Numerical predictions of two-dimensional conduction, convection and radiation heat transfer- part 2", *Int. J. Thermal Science*, Vol. 39, 2000, PP. 323-353.
- [17] Talukdar, P. and Mishra, S. C., "Transient conduction and radiation heat transfer with heat generation in a participating medium using the collapsed dimension method", *J. Numerical Heat Transfer*, Vol. 39, 2001, PP. 79-100.
- [18] Santanu, D., Nagendra, K. and Lakshmisha, N., "Simulation of laminar flow in a three-dimensional lid-driven cavity by lattice Boltzmann method", *Int. J. Numerical Methods for Heat Fluid Flow*, Vol. 19, 2009, PP. 790-815.
- [19] Zhang, T. and Baochang, S., "Lattice Boltzmann simulation of lid-driven flow in trapezoidal cavities", *J. Computers and Fluids*, Vol. 39, 2010, PP. 1977–1989.
- [20] Amiri, H., Mansouri, S. H. and Safavinejad, A., "Combined conductive and radiative heat transfer in an anisotropic scattering participating medium with irregular geometries", *Int. J. Thermal Science*, Vol. 49, 2010, PP. 492-503.
- [21] Jafari, M., Farhadi, M., Sedighi, k. and Fattahi, E., "Numerical simulation of convection heat transfer in a lid-driven cavity with an open side", *J. World Academy of Science Engineering and Technology*, Vol. 59, 2011, PP. 435-439.
- [22] Guermond, J. L. and Mineev, P., "Start-up flow in a three-dimensional lid-driven cavity by means of a massively parallel direction splitting algorithm", *Int. Journal for Numerical Methods in Fluids*, Vol. 45, 2011, PP. 885–899.
- [23] Lari, K., Baneshi, M., Gandjalikhan Nassab, S. A., Komiya, A. and Maruyama, S., "Combined heat transfer of radiation and natural convection in a square cavity containing participating gases", *Int. J. Heat and Mass Transfer*, Vol. 54, 2011, pp. 5087-5099.
- [24] Modest, M. F., *Radiative Heat Transfer*, McGraw-Hill, New York, USA, 2006.